A Novel Lagrange-Multiplier Based Method for Consistent Mesh Tying. [1]

M. L. Parks , L. Romero and P. Bochev *

Computational Mathematics and Algorithms, Sandia National Laboratories
P.O. Box 5800, MS 1320, Albuquerque NM 87185-1320

Abstract

We propose a novel Lagrange-multiplier method for mesh tying in $\mathbb{R}^2$ that passes a linear patch test for subdomains with non-coincident interfaces. This capability is required in contact problems and finite element analysis of complex bodies that were broken into simpler shapes to aid grid generation, and where independent descriptions of a shared curved boundary may not necessarily match. In mortar methods Lagrange multipliers are defined on one of the sides and field continuity is enforced by projecting data from the other side. For some interface configurations, this approach may fail to pass a linear patch test. In our method constraints express equilibrium of weighted field averages on the non-matching interfaces. As a result, selection of master and slave sides, a projection operator, or additional meshing are not required. Numerical results for several prototype mesh tying problems illustrate the attractive computational properties of the new method.

Key words: Mesh tying, non-matching interfaces, finite element methods, Lagrange multipliers

1 Introduction

There are a number of computational techniques and application settings where finite element analysis involves tying together several computational domains. In domain decomposition methods [12], a single finite element mesh is partitioned into subdomains and so every pair of adjoining subdomains shares a common interface. In this case it is well understood how to combine subdomain problems into a single, consistent finite element model.

* Corresponding author.
Email addresses: mlparks@sandia.gov (M. L. Parks), lromero@sandia.gov (L. Romero), pbboche@sandia.gov (P. Bochev).

[1] Sandia is a multiprogram laboratory operated by Sandia Corporation, a Lockheed-Martin Company, for the United States Department of Energy's National Nuclear Security Administration under contract DE-AC-94AL85000.

There are at least two other settings where computation requires interfacing of finite element models on independently meshed domains. One arises in contact problems and another occurs when parts of a complex shape are meshed separately and then must be tied together for the analysis. In the first case, the interface is physical and represents the boundary between two components, such as a threaded screw into a column. In the second case the subdomains are defined to simplify and/or improve efficiency of the meshing process and the boundary is artificially imposed. In either case, however, subdomain grids provide two independent descriptions of the interface between the interacting bodies or the the individual parts of the shape. Unless the interface is linear (in 2D) or planar (in 3D), the two descriptions will not necessarily match, leading to gaps (voids) and overlaps (penetration) between the adjoining domains; see Fig. 1.

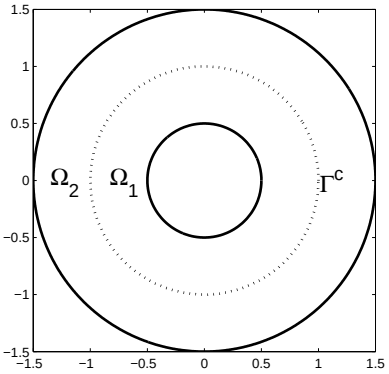

(a) Example domain 1 (annulus).

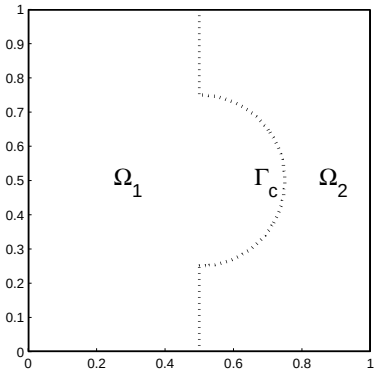

(b) Example domain 2 (unit square).

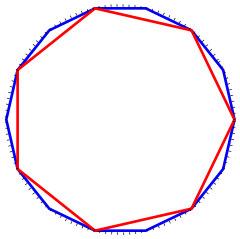

(c) Non-coincident interfaces for example 1.

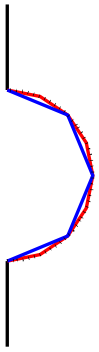

(d) Non-coincident interfaces for example 2.

Fig. 1. Examples of subdomain partitions that will be used throughout the paper. Example 1, based on an example from [7], is an annulus with inner radius $r = 0.5$ and outer radius $r = 1.5$, partitioned by the circular interface boundary at $r = 1.0$. Example 2 is a unit square, partitioned by an interface Γ^c consisting of a semicircle and two straight segments. Subfigures (c) and (d) show typical non-matching interfaces that can result from the independent meshing of the subdomains. In (d), note that the edges discretizing straight segments of the contact boundary are all coincident.

In this paper we consider the task of joining finite element models on two independently meshed subdomains in $\mathbb{R}^2$ that share a curved interface. Several approaches have been proposed to address this problem in both two and three dimensions [7,6,8,3,4,10,11]. As

a rule, the methods considered in these papers extend Lagrange multiplier techniques to non-matching interfaces by selecting a *master* and a *slave* side. For instance, the methods in [6–8] specify Lagrange multipliers on the slave surface and define the constraint equation by projecting displacement fields from the master side into the slave side of the interface. The mesh tying approaches proposed in [3,4,10,11] build additional mesh structures between the slave and master interfaces using tools that range from mesh imprinting to local L^2 projections.

A desirable property of mesh tying algorithms is passing of a linear patch test. Here, by this we mean the ability of the finite element method to recover exactly any globally linear solution of the governing equations, regardless of whether or not the interfaces match. It is well-known that for some interface configurations, mortar methods may fail to pass such a test [3,4]. In this paper we propose a new Lagrange-multiplier based mesh-tying method in $\mathbb{R}^2$ that is guaranteed to pass a linear patch test for virtually any subdomain configuration. Our algorithm is based on equilibration of weighted field averages across the interfaces and so, it does not require selection of a master and a slave sides, projection operators between them, or additional meshing between the subdomains. Because selection of master and slave sides is usually governed by the mesh structure on the interfaces, e.g., the slave is the side that has finer mesh, our algorithm is convenient for cases when mesh resolution between the two interfaces alternates.

To focus on the main ideas of our mesh tying approach we consider solution of the Poisson equation with Dirichlet boundary conditions on two subdomains with non-matching interfaces. To develop the method we start from a standard Lagrange multiplier formulation on subdomains with matching interfaces. The key idea in our approach is to view the Lagrange multiplier as a trace of the normal component $\mathbf{v}\cdot\boldsymbol{n}$ of an $H(\mathrm{div},\Omega)$ vector field, rather than a scalar $H^{-1/2}$ function [2]. This approach is reminiscent of some ideas used in hybridization of mixed methods; see [2]. In the present context it allows us to obtain a natural extension of the saddle-point problem to non-matching interfaces by taking advantage of the fact that the trace of $\mathbf{v}\cdot\boldsymbol{n}$ is well-defined on any curve in the interior of the original domain, which obviates the need for master and slave side designations.

We call the non-matching interfaces between two subdomains *balanced* if and only if the

[2] Throughout the paper we use standard notation and symbols for most function spaces. Given a region D in $\mathbb{R}^2$, the symbols $H^k(D)$, $\|\cdot\|_{k,D}$, $|\cdot|_{k,D}$ and $(\cdot,\cdot)_{k,D}$ denote the Sobolev space of all square integrable functions functions with square integrable derivatives up to order k, and the standard Sobolev norm, seminorm and inner product, respectively. As usual, instead of $H^0(D)$ we write $L^2(D)$, $H^1_0(D)=\{v\in H^1(D)\,|\,v=0 \text{ on } \partial D\}$ and $L^2_0(D)=\{q\in L^2(D)\,|\,\int_D q\,dx=0\}$. Spaces of vector valued functions are denoted by bold-face notation so that $\mathbf{H}^1(D)$ is the space of vector-valued functions with components $H^1(D)$. The space $H(\mathrm{div},D)$ is defined as

$$H(\mathrm{div},D)=\{\mathbf{v}\in\mathbf{L}^2(D)\,|\,\nabla\cdot\mathbf{v}\in L^2(D)\}$$

with norm $\|\mathbf{v}\|_{H(\mathrm{div,D})}=\left(\|\mathbf{v}\|^2_{0,D}+\|\nabla\cdot\mathbf{v}\|^2_{0,D}\right)^{1/2}$.
The subspace of H^1 functions that vanish on a subset $\Gamma\subset\partial D$ is $H^1_\Gamma(D)$. The trace of a function $\phi\in H^1(D)$ on a subset $\Gamma\subset\partial D$ belongs to the space $H^{1/2}(\Gamma)$. Extensions by zero of functions in $H^{1/2}(\Gamma)$ to $H^{1/2}(\partial D)$ are in the space $H^{1/2}_{00}(\Gamma)$. The dual of this space is $H^{-1/2}(\Gamma)$; see [12, p.342], and $\langle\cdot,\cdot\rangle_\Gamma$ denotes the duality pairing.

areas of the void and overlap regions defined by them are equal. We show that a necessary condition to pass a linear patch test is to have balanced interfaces. To meet this condition we use a simple procedure to perturb the nodes until void and overlap areas cancel. It is important to note that the interface balancing step remains a virtual operation that uses the new node positions to modify the assembly matrices, but does not physically change the interfaces.

The final step in our algorithm is selection of finite element approximation spaces for the traces of $\mathbf{v} \cdot \boldsymbol{n}$. We assume that the interface boundary is piecewise smooth and consist of a finite number of smooth segments. The discrete Lagrange multiplier space is defined in three stages. At the first stage we include functions needed to represent exactly the flux of any globally linear function across the interfaces. At the second stage we enrich this set by functions that are piecewise polynomials *with respect to the discrete interface segments* that approximate the smooth segments of the true interface. These polynomials are parameterized by the arc length of the segments and their degree depends on the edge count in the discrete segments. The final, third stage, is to select a subspace of *linear patch test compatible* discrete multipliers.

In the case of coincident interfaces our method recovers a mortar-like method in which discrete Lagrange multipliers are piecewise polynomials but with respect to the segmentation of the true interface into a finite number of smooth segments. In the extreme case when each segment corresponds to an element edge we recover a classical dual Lagrange multiplier method.

We have organized the paper as follows. The model equations, the interface problem for non-coincident interfaces and its constrained optimization formulation are introduced in §2. There we also prove that the resulting saddle-point variational problem is well-posed and derive a necessary condition for a linear patch test. The finite element mesh tying method is introduced in §3. This section formulates the interface balancing procedure and explains how the finite element spaces for the displacements and the Lagrange multipliers are defined. Numerical studies of the new mesh-tying method are presented in §4 and §5 summarizes our findings and future research directions.

2 Statement of the interface problem

Let Ω be a simply connected bounded open domain in $\mathbb{R}^2$ with a sufficiently smooth boundary Γ. We consider the Poisson equation with Dirichlet boundary conditions:

$$-\triangle\phi = f \text{ in } \Omega \quad \text{and} \quad \phi = g \text{ on } \Gamma\,, \tag{1}$$

where $f \in L^2(\Omega)$ and $g \in H^{1/2}(\Gamma)$ are given functions. For clarity we will formulate our mesh-tying method in the case when Ω consists of two subdomains Ω_1 and Ω_2. We assume that

$$\Omega_1 \cup \Omega_2 \subset \Omega\,; \quad \partial\Omega_i = \Gamma_i \cup \Gamma_i^c\,; \quad \Gamma_1 \cup \Gamma_2 = \Gamma \quad \text{and} \quad \Gamma_1 \cap \Gamma_2 = \emptyset\,,$$

where $\Gamma_i = \partial\Omega_i \cap \partial\Omega$ and Γ_i^c are the *interface* boundaries. We allow one of Γ_i to be empty; this corresponds to one of the subdomains being a proper subset of Ω. Note that if $\Gamma_i \neq \emptyset$ for $i = 1, 2$, our assumptions imply that Γ_1^c and Γ_2^c have common endpoints; see subfigure (b) in Fig. 1. For convenience, we will assume that this is also the case when one of Γ_i is

empty.

Furthermore, we assume that the *overlap* and *void* regions, defined by

$$\Omega_o = \Omega_1 \cap \Omega_2 \quad \text{and} \quad \Omega_v = \Omega/(\Omega_1 \cup \Omega_2)\,,$$

respectively, are both contained in Ω and consist of a finite number of connected components; see Fig. 1.

We call a configuration where $\Gamma^c = \Gamma_1^c = \Gamma_2^c$ a *matching* interface problem for (1). Accordingly, a configuration where $\Gamma_1^c \neq \Gamma_2^c$ is a *non-matching* interface problem for the Poisson equation. In the former case Ω_o and Ω_v are empty. For a non-matching interface problem at least one of Ω_o or Ω_v is non-empty.

Suppose that σ is closed curve in $\mathbb{R}^2$ that encloses a contractible region Σ. The choice of a unit normal $\boldsymbol{n}_\sigma$ on σ endows Σ with orientation. By $A(\Sigma)$ we denote the oriented area of Σ, i.e., $A(\Sigma)$ is positive if $\boldsymbol{n}_\sigma$ coincides with the direction of the outer normal on $\partial\Sigma$ and $A(\Sigma)$ is negative if $\boldsymbol{n}_\sigma$ points inward. It is easy to see that all components of Ω_o are oriented *positively*, whereas the components of Ω_v are oriented *negatively*. Let

$$\Omega_c = \Omega_o \cup \Omega_v\,.$$

We call the non-coincident interface *balanced* if $A(\Omega_c) = 0$. Note that

$$A(\Omega_c) = A(\Omega_o) + A(\Omega_v)\,,$$

and so an interface is balanced if and only if the void and overlap areas cancel each other. Another interpretation of the balanced interface condition can be derived from the identity $A(\Omega_c) = A(\Omega_1) + A(\Omega_2) - A(\Omega)$. In this case, we see that an interface is balanced if and only if the total area of the subdomains matches the area of the original domain.

To state formally the interface problem for (1) we introduce the tensor product space

$$\mathbf{H} = \{\overline{\phi} = (\phi_1, \phi_2)\,|\,\phi_i \in H^1(\Omega_i);\ i = 1, 2\}\,,$$

equipped with norm

$$\|\overline{\phi}\|_{\mathbf{H}} = \left(\|\phi_1\|_{1,\Omega_1}^2 + \|\phi_2\|_{1,\Omega_2}^2\right)^{1/2}\,,$$

its proper subspace

$$\mathbf{H}_0 = \{\overline{\phi} \in \mathbf{H}\,|\,\phi_i = 0 \text{ on } \Gamma_i;\ i = 1, 2\}\,,$$

and the affine space

$$\mathbf{H}_g = \{(\phi_1, \phi_2) \in \mathbf{H}\,|\,\phi_i = g \text{ on } \Gamma_i;\ i = 1, 2\}\,,$$

along with the trace space $H_{00}^{1/2}(\Gamma_i^c)$, and its dual $H^{-1/2}(\Gamma_i^c)$. For simplicity we denote the duality pairing between $H_{00}^{1/2}(\Gamma_i^c)$ and $H^{-1/2}(\Gamma_i^c)$ by $\langle\cdot,\cdot\rangle_i$. Given $\overline{\phi} \in \mathbf{H}_0$, the trace of ϕ_i on Γ_i^c belongs to $H_{00}^{1/2}(\Gamma_i^c)$. The normal component $\mathbf{v} \cdot \boldsymbol{n}_i$ of a vector field $\mathbf{v} \in H(\mathrm{div}, \Omega)$ on Γ_i^c is in the dual space $H^{-1/2}(\Gamma_i^c)$.

2.1 A matching interface problem for the Poisson equation

The case of matching interfaces $\Gamma^c = \Gamma_1^c = \Gamma_2^c$ corresponds to $\overline{\Omega} = \overline{\Omega_1 \cup \Omega_2}$ and $\Omega_1 \cap \Omega_2 = \emptyset$ and so, it is the familiar non-overlapping domain decomposition formulation of (1): find $\overline{\phi} \in \mathbf{H}_g$ such that

$$-\triangle \phi_i = f \quad \text{in } \Omega_i \quad \text{and} \quad \phi_i = g \quad \text{on } \Gamma_i \tag{2}$$

subject to the interface conditions

$$\nabla \phi_1 \cdot \boldsymbol{n}_1 + \nabla \phi_2 \cdot \boldsymbol{n}_2 = 0 \quad \text{and} \quad \phi_1 - \phi_2 = 0 \quad \text{on } \Gamma^c\,. \tag{3}$$

Problem (2) is equivalent to the constrained optimization problem

$$\inf_{\overline{\psi} \in \mathbf{H}} \sum_{i=1}^{2} \frac{1}{2} \int_{\Omega_i} |\nabla \psi_i|^2 \, dx - \int_{\Omega_i} f \psi_i \, dx \quad \text{subject to } \psi_1 = \psi_2 \text{ on } \Gamma^c. \tag{4}$$

A standard approach in the domain decomposition literature is to enforce the second (field continuity) constraint in (3) weakly by using Lagrange multipliers from the space $H^{-1/2}(\Gamma^c)$. This transforms (4) into a saddle point problem; see [5,7,8]. Such a choice is perfectly admissible for matching interfaces but is prone to difficulties when $\Gamma_1^c \neq \Gamma_2^c$ because the approximation of $H^{-1/2}(\Gamma^c)$ cannot be "split" between the two distinct interfaces. The solution in this case is to approximate $H^{-1/2}(\Gamma^c)$ on only one of the interfaces (usually called a *slave* side) and to impose (3) weakly by projecting fields from the master onto the slave side.

In this paper we adopt an alternative approach in which Lagrange multipliers are vector fields $\mathbf{w}$ from $H(\mathrm{div}, \Omega)$ and weak continuity is enforced by using their normal components $\mathbf{w} \cdot \boldsymbol{n}$ on the interface. This choice, originally considered in the context of hybridization for mixed finite element methods; see [2, p.140-142], transforms (4) into the saddle-point problem

$$\inf_{\overline{\psi} \in \mathbf{H}_g} \sup_{\mathbf{w} \in H(\mathrm{div}, \Omega)} \left(\sum_{i=1}^{2} \frac{1}{2} \int_{\Omega_i} |\nabla \psi_i|^2 \, dx - \int_{\Omega_i} f \psi_i \, dx - \int_{\Gamma_c} (\mathbf{w} \cdot \boldsymbol{n}) \psi_i \, dS \right). \tag{5}$$

We recall that the trace $\mathbf{v} \mapsto \mathbf{v} \cdot \boldsymbol{n}$ is a well-defined mapping from $H(\mathrm{div}, \Omega)$ into $H^{-1/2}(\Gamma^c)$; see [9, Theorem 2.5, p.27] and so, for a single interface Γ^c the two approaches are completely equivalent. However, (5) has an advantage over the standard approach when the interfaces do not match because the trace of $\mathbf{v} \cdot \boldsymbol{n}$ remains well defined on any curve inside Ω.

2.2 A non-matching interface problem of the Poisson equation

Consider now the case when $\Gamma_1^c \neq \Gamma_2^c$. The strong problem (2)-(3) does not admit a natural extension to this case and so, to obtain a formal statement of the interface problem we proceed with the weak saddle-point equation (5).

By assumption $\Gamma_i^c \subset \Omega$, $i = 1, 2$ and, as a result, for any $\mathbf{w} \in H(\mathrm{div}, \Omega)$ the trace $\mathbf{w} \cdot \boldsymbol{n}_i$ is well-defined in $H^{-1/2}(\Gamma_i^c)$. Therefore, the saddle-point problem

$$\inf_{\overline{\psi} \in \mathbf{H}_g} \sup_{\mathbf{w} \in H(\mathrm{div}, \Omega)} \sum_{i=1}^{2} \left(\frac{1}{2} \int_{\Omega_i} |\nabla \psi_i|^2 \, dx - \int_{\Omega_i} f \psi_i \, dx - \int_{\Gamma_i^c} (\mathbf{w} \cdot \boldsymbol{n}) \psi_i \, dS \right) \tag{6}$$

is a generalization of (5) for non-matching interfaces, where the integral over Γ^c in (5) has been replaced in (6) by two separate integrals over Γ_1^c and Γ_2^c. Moreover, because $\mathbf{w}\cdot\boldsymbol{n}$ is defined on both interfaces there's no need to distinguish between a master and a slave boundary.

The Euler-Lagrange equation of (6) is to seek $\phi \in \mathbf{H}_g$ and $\mathbf{v} \in H(\mathrm{div},\Omega)$ such that

$$\begin{aligned}
(\nabla\phi_1,\nabla\psi_1) \qquad\qquad & -\langle \mathbf{v}\cdot\boldsymbol{n}_1,\psi_1\rangle_1 = (f,\psi_1) \quad && \forall\psi_1 \in H^1_{\Gamma_1}(\Omega_1)\\
(\nabla\phi_2,\nabla\psi_2) \quad & -\langle \mathbf{v}\cdot\boldsymbol{n}_2,\psi_2\rangle_2 = (f,\psi_2) \quad && \forall\psi_2 \in H^1_{\Gamma_2}(\Omega_2)\\
\langle \mathbf{w}\cdot\boldsymbol{n}_1,\phi_1\rangle_1 + \langle \mathbf{w}\cdot\boldsymbol{n}_2,\phi_2\rangle_2 \qquad & = 0 && \forall\mathbf{w} \in H(\mathrm{div},\Omega)
\end{aligned} \tag{7}$$

The last equation in (7) generalizes the usual weak continuity constraint on a single interface to the case of non-matching interfaces. It can be interpreted as enforcing an equilibrium of the weighted field averages along the two interfaces.

To show that (7) is a well-posed problem we use the abstract saddle-point theory in [1]. In order to avoid tedious technical details we restrict attention to homogeneous Dirichlet boundary conditions. To cast (7) into the framework of [1] we define the bilinear forms

$$a(\overline{\phi},\overline{\psi}) = \sum_{i=1}^{2}\int_{\Omega_i}\nabla\phi_i\cdot\nabla\psi_i\,dx\,; \quad b(\overline{\psi},\mathbf{w}) = -\sum_{i=1}^{2}\int_{\Gamma_i^c}(\mathbf{w}\cdot\boldsymbol{n})\psi_i\,dS\,, \tag{8}$$

and the spaces

$$\begin{aligned}
\mathbf{Z} &= \{\overline{\psi}\in\mathbf{H}_0 \,|\, b(\overline{\psi},\mathbf{w}) = 0\ \forall\mathbf{w}\in H(\mathrm{div},\Omega)\}\,,\\
\mathbf{Z}' &= \{\mathbf{w}\in H(\mathrm{div},\Omega) \,|\, b(\overline{\psi},\mathbf{w}) = 0\ \forall\overline{\psi}\in\mathbf{H}_0\}\,.
\end{aligned} \tag{9}$$

The following theorem contains the main result of this section.

Theorem 1 *For any $f \in L^2(\Omega)$ and $g = 0$ problem (7) has a unique solution $(\overline{\phi},\mathbf{v}) \in \mathbf{H}_0 \times H(\mathrm{div},\Omega)/\mathbf{Z}'$.*

The proof of the theorem relies on an auxiliary result presented in the next lemma.

Lemma 1 *Let $\mathbf{Z}'$ be the space defined in (9). For any $\mathbf{v}\in H(\mathrm{div},\Omega)$*

$$\frac{1}{2}\|\mathbf{v}\|_{H(\mathrm{div},\Omega)/\mathbf{Z}'} \le \|\mathbf{v}\cdot\boldsymbol{n}\|_{-1/2,\Gamma_1^c} + \|\mathbf{v}\cdot\boldsymbol{n}\|_{-1/2,\Gamma_2^c}\,. \tag{10}$$

Proof. We need to show that

$$\frac{1}{2}\inf_{\mathbf{v}_0\in\mathbf{Z}'}\|\mathbf{v}+\mathbf{v}_0\|_{H(\mathrm{div},\Omega)} \le \|\mathbf{v}\cdot\boldsymbol{n}\|_{-1/2,\Gamma_1^c} + \|\mathbf{v}\cdot\boldsymbol{n}\|_{-1/2,\Gamma_2^c}\,.$$

For this purpose we extend an idea from Corollary 2.8 [9, p.28]. Without loss of generality we may assume that Ω_v consists of a single connected component and that $\Omega_c = \Omega_v$. Let

$\phi_i \in H^1_{\Gamma_i}(\Omega_i)$ and $\phi_c \in H^1(\Omega_c)$ be the unique solutions of

$$\begin{cases} -\triangle\phi_i + \phi_i = 0 \text{ in } \Omega_i \\ \nabla\phi_i \cdot \boldsymbol{n} = \mathbf{v}\cdot\boldsymbol{n} \text{ on } \Gamma_i^c \\ \phi_i = 0 \text{ on } \Gamma_i \end{cases} i = 1,2 \quad \text{and} \quad \begin{cases} -\triangle\phi_c + \phi_c = 0 \text{ in } \Omega_c \\ \nabla\phi_c \cdot \boldsymbol{n} = \mathbf{v}\cdot\boldsymbol{n} \text{ on } \Gamma^c \end{cases},$$

respectively. Then

$$\|\phi_i\|^2_{1,\Omega_i} = \langle \mathbf{v}\cdot\boldsymbol{n}, \phi_i\rangle_{\Gamma_i^c} \quad \text{and} \quad \|\phi_c\|^2_{1,\Omega_c} = \langle \mathbf{v}\cdot\boldsymbol{n}, \phi_c\rangle_{\Gamma^c}$$

and so, it is not hard to see that

$$\|\phi_i\|_{1,\Omega_i} \le \|\mathbf{v}\cdot\boldsymbol{n}\|_{-1/2,\Gamma_i^c} \quad \text{and} \quad \|\phi_c\|_{1,\Omega_c} \le \sum_{i=1}^{2} \|\mathbf{v}\cdot\boldsymbol{n}\|_{-1/2,\Gamma_i^c}\,.$$

If we define $\hat{\mathbf{v}}_i = \nabla\phi_i$, $i = 1,2$ and $\hat{\mathbf{v}}_c = \nabla\phi_c$, then $\nabla\cdot\hat{\mathbf{v}}_i = \phi_i$, $\nabla\cdot\hat{\mathbf{v}}_C = \phi_c$ and

$$\|\hat{\mathbf{v}}_i\|_{H(\mathrm{div},\Omega_i)} = \|\phi_i\|_{1,\Omega_i} \quad \text{and} \quad \|\hat{\mathbf{v}}_c\|_{H(\mathrm{div},\Omega_c)} = \|\phi_c\|_{1,\Omega_c}$$

and so

$$\sum_{i=1}^{2} \|\hat{\mathbf{v}}_i\|_{H(\mathrm{div},\Omega_i)} + \|\hat{\mathbf{v}}_c\|_{H(\mathrm{div},\Omega_c)} \le 2\sum_{i=1}^{2} \|\mathbf{v}\cdot\boldsymbol{n}\|_{-1/2,\Gamma_i^c}\,. \tag{11}$$

To complete the proof, note that the function

$$\hat{\mathbf{v}} = \begin{cases} \hat{\mathbf{v}}_i \text{ in } \Omega_i \\ \hat{\mathbf{v}}_c \text{ in } \Omega_c \end{cases}$$

belongs to $H(\mathrm{div},\Omega)$ and can be written as $\mathbf{v} + \hat{\mathbf{v}}_0$ where $\hat{\mathbf{v}}_0 \in \mathbf{Z}'$. The lemma follows from

$$\|\mathbf{v} + \hat{\mathbf{v}}_0\|_{H(\mathrm{div},\Omega)} = \|\hat{\mathbf{v}}\|_{H(\mathrm{div},\Omega)} \le \sum_{i=1}^{2} \|\hat{\mathbf{v}}_i\|_{H(\mathrm{div},\Omega_i)} + \|\hat{\mathbf{v}}_c\|_{H(\mathrm{div},\Omega_c)}$$

and the upper bound in (11). □

Proof of Theorem 1. To apply the abstract theory of [1] we need to show that $a(\cdot,\cdot)$ is coercive on $\mathbf{Z}$ and that $b(\cdot,\cdot)$ satisfies the inf-sup condition

$$\sup_{\overline{\psi}\in\mathbf{H}_0} \frac{b(\overline{\psi},\mathbf{w})}{\|\overline{\psi}\|_{\mathbf{H}}} \ge \gamma\|\mathbf{w}\|_{H(\mathrm{div},\Omega)/\mathbf{Z}'} \quad \forall \mathbf{w} \in H(\mathrm{div},\Omega)\,, \tag{12}$$

with γ a positive real constant. It is easy to see that for any $\overline{\phi} \in \mathbf{H}_0$

$$a(\overline{\phi},\overline{\phi}) = \|\phi_1\|^2_{1,\Omega_1} + \|\phi_2\|^2_{1,\Omega_2} = \|\overline{\phi}\|^2_{\mathbf{H}}\,,$$

and so $a(\cdot,\cdot)$ is coercive on all of $\mathbf{H}$. Thus, the first condition of the abstract theory is trivially

satisfied. To check (12) recall that components of $\overline{\psi} \in \mathbf{H}_0$ have traces in $H^{1/2}_{00}(\Gamma^c_i)$ and so

$$\sup_{\overline{\psi}\in\mathbf{H}_0} \frac{b(\overline{\psi},\mathbf{w})}{\|\overline{\psi}\|_{\mathbf{H}}} = \sup_{\overline{\psi}\in\mathbf{H}_0} \frac{\sum_{i=1}^{2}\langle\psi_i, \mathbf{w}\cdot\boldsymbol{n}\rangle_i}{\|\psi_1\|_{1,\Omega_1}+\|\psi_2\|_{1,\Omega_2}} = \sum_{i=1}^{2}\|\mathbf{w}\cdot\boldsymbol{n}\|_{-1/2,\Gamma^c_i}\,.$$

The inf-sup condition (12) follows from (10) in Lemma 1. □

Theorem 1 shows that (6), respectively (7) are well posed problems despite the fact that Γ^c_1 does not match Γ^c_2. However, Theorem 1 does not guarantee that (7) will admit as solutions restrictions of a globally linear solution of (1) and its constant gradient. More precisely, if $\phi^L = ax + by + c$, $f = -\triangle\phi^L = 0$ and $g = \phi^L|_\Gamma$, there is no guarantee that $(\overline{\phi}^L, \mathbf{v})$ where $\phi^L_1 = \phi^L|_{\Omega_1}$, $\phi^L_2 = \phi^L|_{\Omega_2}$ and $\mathbf{v} = \nabla\phi^L$ will be a solution of (7). The following lemma shows that balanced interfaces are a necessary condition for this to happen.

Lemma 2 *Let A_c denote the oriented area of Ω_c; $\phi^L = ax + by + c$, $\phi^L_i = \phi^L|_{\Omega_i}$, and $\overline{\phi}^L = (\phi^L_1, \phi^L_2)$. A necessary condition for (7) to admit $(\overline{\phi}^L, \nabla\overline{\phi}^L)$ as a solution is $A_c = 0$.*

Proof. Assume that f and g are defined as above. Setting $\mathbf{v} = \nabla\phi^L$ in the first two equations of (7) yields

$$\begin{aligned}
\left(\nabla\phi^L_1, \nabla\psi_1\right) - \langle\mathbf{v}\cdot\boldsymbol{n}_1, \psi_1\rangle_1 = \langle\nabla\phi^L_1\cdot\boldsymbol{n}_1, \psi_1\rangle_1 - \langle\mathbf{v}\cdot\boldsymbol{n}_1, \psi_1\rangle_1 = 0 \quad \forall\psi_1 \in H^1_{\Gamma_1}(\Omega_1)\\
\left(\nabla\phi^L_2, \nabla\psi_2\right) - \langle\mathbf{v}\cdot\boldsymbol{n}_2, \psi_2\rangle_2 = \langle\nabla\phi^L_2\cdot\boldsymbol{n}_2, \psi_2\rangle_2 - \langle\mathbf{v}\cdot\boldsymbol{n}_2, \psi_2\rangle_2 = 0 \quad \forall\psi_2 \in H^1_{\Gamma_2}(\Omega_2)
\end{aligned}$$

Hence, the first two equations will be always satisfied by the pair $(\overline{\phi}^L, \nabla\overline{\phi}^L)$. In general, this pair may not solve the third equation in (7) for *all* possible choices of $\mathbf{w} \in H(\mathrm{div}, \Omega)$. However, we seek a necessary condition that will work in conjunction with a piecewise polynomial approximation of $H(\mathrm{div}, \Omega)$. To obtain such a condition note that if $(\overline{\phi}^L, \nabla\overline{\phi}^L)$ were to solve (7), then at least, the last equation must hold for the choice $\mathbf{w} = \nabla\phi^L$. Therefore, we must have the identity

$$\langle\nabla\phi^L\cdot\boldsymbol{n}_1, \phi^L_1\rangle_1 + \langle\nabla\phi^L\cdot\boldsymbol{n}_2, \phi^L_2\rangle_2 = 0$$

Because

$$\nabla\phi^L = a\begin{pmatrix}1\\0\end{pmatrix} + b\begin{pmatrix}0\\1\end{pmatrix} = a\mathbf{e}_1 + b\mathbf{e}_2$$

this identity will hold true if and only if

$$\left.\begin{aligned}
\langle\mathbf{e}_i\cdot\boldsymbol{n}_1, 1\rangle_1 + \langle\mathbf{e}_i\cdot\boldsymbol{n}_2, 1\rangle_2 = 0\\
\langle\mathbf{e}_i\cdot\boldsymbol{n}_1, x\rangle_1 + \langle\mathbf{e}_i\cdot\boldsymbol{n}_2, x\rangle_2 = 0\\
\langle\mathbf{e}_i\cdot\boldsymbol{n}_1, y\rangle_1 + \langle\mathbf{e}_i\cdot\boldsymbol{n}_2, y\rangle_2 = 0
\end{aligned}\right\} \quad \text{for } i = 1, 2\,.$$

Let $\boldsymbol{n}_c$ be the outer normal to $\Gamma_c = \partial\Omega_c$. Definition of Ω_c implies that

$$\langle\mathbf{w}\cdot\boldsymbol{n}_c, \phi\rangle_{\Gamma_c} = \langle\mathbf{w}\cdot\boldsymbol{n}_1, \phi\rangle_1 + \langle\mathbf{w}\cdot\boldsymbol{n}_2, \phi\rangle_2\,,$$

and so, using the Divergence Theorem

$$\langle \mathbf{e}_i \cdot \boldsymbol{n}_1, 1\rangle_1 + \langle \mathbf{e}_i \cdot \boldsymbol{n}_2, 1\rangle_2 = \int_{\Omega_c} \nabla \cdot \mathbf{e}_i \, dx = 0$$

$$\langle \mathbf{e}_1 \cdot \boldsymbol{n}_1, y\rangle_1 + \langle \mathbf{e}_1 \cdot \boldsymbol{n}_2, y\rangle_2 = \int_{\Omega_c} \nabla \cdot y\mathbf{e}_1 \, dx = 0$$

$$\langle \mathbf{e}_2 \cdot \boldsymbol{n}_1, x\rangle_1 + \langle \mathbf{e}_2 \cdot \boldsymbol{n}_2, x\rangle_2 = \int_{\Omega_c} \nabla \cdot x\mathbf{e}_2 \, dx = 0$$

$$\langle \mathbf{e}_1 \cdot \boldsymbol{n}_1, x\rangle_1 + \langle \mathbf{e}_1 \cdot \boldsymbol{n}_2, x\rangle_2 = \int_{\Omega_c} \nabla \cdot x\mathbf{e}_1 \, dx = A_c$$

$$\langle \mathbf{e}_2 \cdot \boldsymbol{n}_1, y\rangle_1 + \langle \mathbf{e}_2 \cdot \boldsymbol{n}_2, y\rangle_2 = \int_{\Omega_c} \nabla \cdot y\mathbf{e}_2 \, dx = A_c$$

Therefore, the constraint equation in (7) is satisfied iff $A_c = 0$. This proves the lemma. □

We note that Lemma 2 only establishes a minimal requirement for $(\overline{\phi}^L, \nabla\overline{\phi}^L)$ to be a solution of (7) and in no way implies that this pair *is a solution* of the weak problem. Theorem 1 asserts existence of a solution to (7), however, it does not assert that $(\overline{\phi}^L, \nabla\overline{\phi}^L)$ will be recovered. In other words, even if the area discrepancy is zero, we are not guaranteed that (7) will admit $(\overline{\phi}^L, \nabla\overline{\phi}^L)$ as a solution. However, as we shall see in the next section, a finite element solution of (7) can be formulated in a way that will always recover linear solutions.

3 Finite element solution of the mesh-tying problem

In this section we use the saddle-point problem (7) to formulate a finite element method for mesh tying. In this context Ω_1 and Ω_2 represent two independently meshed versions of two subdomains that share a common boundary Γ^c and the non-matching interfaces result from approximation of Γ^c by, e.g., polygons. Thus, without loss of generality we may assume that Γ^c and its approximations Γ_1^c and Γ_2^c are within $O(h)$ of each other in the following sense: there exists a finite number of points $\{\boldsymbol{x}_i\}_{i=1}^n$, $\boldsymbol{x}_i \in \Gamma^c$ and a positive constant μ such that

$$\Gamma_i^c \subset \bigcup_{i=1}^{n} B(\boldsymbol{x}_i, \mu h) \tag{13}$$

where h is a measure of the grid size and $B(\boldsymbol{x}, r)$ is a ball of radius r centered at $\boldsymbol{x}$.

In what follows we consider piecewise smooth interfaces Γ^c that consist of a finite number of smooth segments σ^s; $s = 1, \ldots, n_\sigma$; see Fig.2. Thanks to (13) we can assume that

$$\Gamma_i^c = \bigcup_{s=1}^{n_\sigma} \sigma_i^s \quad \text{and} \quad \sigma_i^s \cap \sigma_i^r = \emptyset \quad \text{for } r \neq s\,,$$

where σ_i^s approximates σ^s.

To emphasize the fact that the Ω_i are defined by a finite element partition we write Ω_i^h. We assume that the Dirichlet boundary Γ_i is polygonal and so it is meshed exactly, that is, $\Gamma_i = \Gamma_i^h$, where Γ_i^h is the Dirichlet boundary of Ω_i^h. $\mathcal{N}(\overline{\Omega}_i)$ is the set of all grid nodes $\mathbf{x}_i$ in

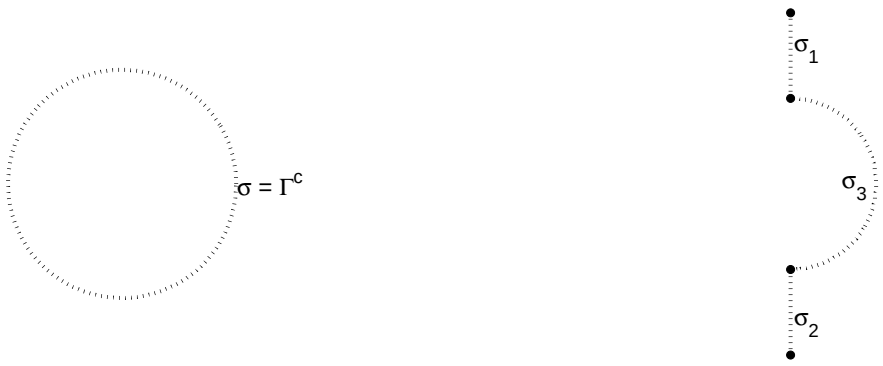

(a) The contact interface for example 1.

(b) The contact interface for example 2. In this example, $\Gamma^c = \sigma_1 \cup \sigma_2 \cup \sigma_3$.

Fig. 2. Contact boundaries for each example broken into segments.

Ω_i^h and $\mathcal{N}(\Omega_i)$ is the set of all interior nodes in Ω_i^h. $\mathcal{N}(\Gamma_i^c)$ is the set of all nodes on interface boundary Γ_i^c, $\mathcal{N}(\Gamma_i)$ is the set of all nodes on the Dirichlet boundary Γ_i.

Our goal is to define a finite element method for (7) that, as a minimal requirement, passes a linear patch test. From Lemma 2 we know that a necessary condition for this is to have a balanced interface. In the next section we formulate a simple procedure that sets $A_c = 0$ by perturbing interface nodes. Then, we proceed to define the finite element spaces for the displacements $\overline{\phi} \in \mathbf{H}_g$ and for the normal components of the Lagrange multiplier fields $\mathbf{w} \in H(\mathrm{div}, \Omega)$.

3.1 Interface balancing procedure

Let $\{\boldsymbol{x}_i^1, \ldots, \boldsymbol{x}_i^{k_i}\} = \mathcal{N}(\Gamma_i^c)/\mathcal{N}(\Gamma_i^c) \cap \mathcal{N}(\Gamma_i)$ denote all nodes on Γ_i^c that are not on the Dirichlet boundary Γ_i. We seek perturbations $\{\delta\boldsymbol{x}_i^1, \ldots, \delta\boldsymbol{x}_i^{k_i}\}$ such that $A_c = 0$ on the perturbed subdomains. Let $\delta\Gamma_i^c$ denote the perturbed interface and define the functions

$$L_i(\delta\boldsymbol{x}_i^1, \ldots, \delta\boldsymbol{x}_i^{k_i}) = \langle \mathbf{e}_1 \cdot \boldsymbol{n}_i, x \rangle_{\delta\Gamma_i^c}; \quad i = 1, 2\,.$$

From the formula

$$A_c = \langle \mathbf{e}_1 \cdot \boldsymbol{n}_1, x \rangle_1 + \langle \mathbf{e}_1 \cdot \boldsymbol{n}_2, x \rangle_2 = \langle \mathbf{e}_2 \cdot \boldsymbol{n}_1, y \rangle_1 + \langle \mathbf{e}_2 \cdot \boldsymbol{n}_2, y \rangle_2\,,$$

established in Lemma 2, it follows that $L_1(\delta\boldsymbol{x}_1^1, \ldots, \delta\boldsymbol{x}_1^{k_1}) + L_2(\delta\boldsymbol{x}_2^1, \ldots, \delta\boldsymbol{x}_2^{k_2}) = A_c$. Therefore, to determine $\{\delta\boldsymbol{x}_i^1, \ldots, \delta\boldsymbol{x}_i^{k_i}\}$ we solve the equation

$$\sum_{i=1}^{2} L_i(\delta\boldsymbol{x}_i^1, \ldots, \delta\boldsymbol{x}_i^{k_i}) = 0\,. \tag{14}$$

The problem (14) is underdetermined. In a least-squares sense, we choose the solution that minimizes the 2-norm of the vector of perturbations. Also note that L_i are quadratic functions of the nodal perturbations, so a single Newton step would give the exact perturbation. After the nodal perturbations are determined, they are stored for subsequent use to modify computation of the affected entries in the subdomain stiffness matrices.

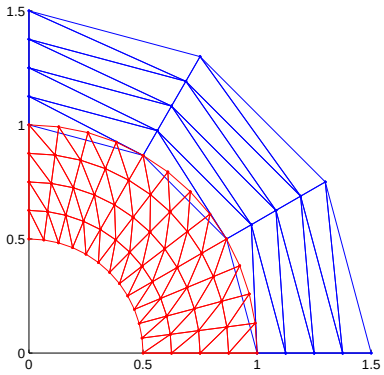

(a) Part of the example 1 mesh before perturbation of Γ^c.

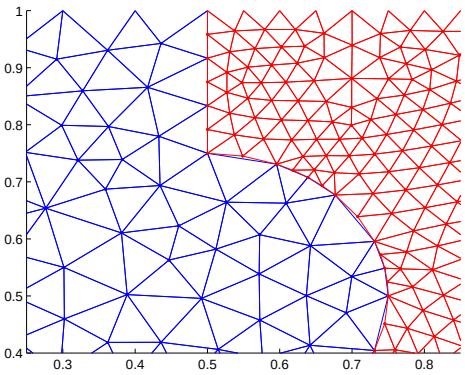

(b) Part of the example 2 mesh before perturbation of Γ^c.

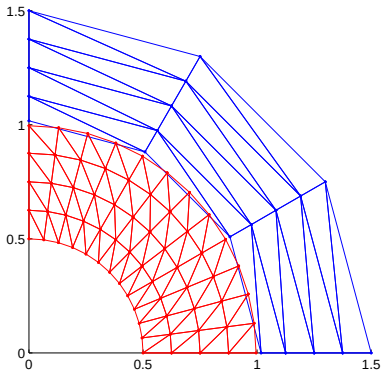

(c) Part of the example 1 mesh after perturbation of Γ^c.

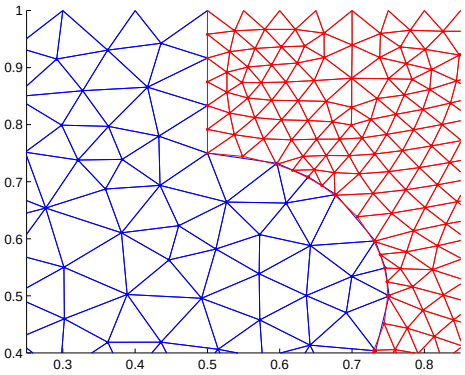

(d) Part of the example 2 mesh after perturbation of Γ^c.

Fig. 3. Example finite element meshes for domains 1 and 2 both before and after the balancing perturbation.

Figure 3 shows an example of a non-matching interface with $A_c \neq 0$ and the balanced interface after the application of the balancing procedure. The plots in the bottom row of this figure show the perturbed positions of the interface nodes in order to demonstrate the balanced interface. In the actual implementation of the method, geometry data for the interface nodes is not changed; instead, for all elements that have edges on the interfaces we compute the entries of the element stiffness matrix by using the perturbed coordinates. Note also from that even if certain boundary nodes were coincident before perturbation, they are generally not coincident afterwards. This can be seen, for example, by comparing figures 3(a) and 3(c). Additionally, note that perturbations along straight interface segments, (see segments σ_1 and σ_2 in figures 2(b) and 3(b)/3(d)) will be zero because $A_c = 0$ initially. In generally, perturbations are only required for curved boundaries.

3.2 Finite element spaces

For brevity we discuss selection of finite element spaces only for partitions Ω_i^h consisting of triangular elements T. We assume that the interface has already been balanced, so through-

out this section $A_c = 0$.

3.2.1 Approximation of the displacement fields

Given an element $T \in \Omega_i^h$, let $\mathcal{P}_1(T)$ denote the space of all linear polynomials on T. The standard C^0 piecewise linear Lagrangian space on Ω_i^h is defined by

$$S^h(\Omega_i^h) = \left\{ \phi_i^h \in C^0(\Omega_i^h) \mid \phi_i^h|_T \in \mathcal{P}_1(T) \quad \forall T \in \Omega_i^h \right\} .$$

For problems with inhomogeneous Dirichlet boundary conditions we use the space

$$S_g^h(\Omega_i^h) = \left\{ \phi_i^h \in C^0(\Omega_i^h) \mid \phi_i^h|_T \in \mathcal{P}_1(T) \quad \forall T \in \Omega_i^h \ \text{ and } \ \phi_i^h(\boldsymbol{x}) = g(\boldsymbol{x}) \ \forall \boldsymbol{x} \in \mathcal{N}(\Gamma_i) \right\}$$

whose elements are constrained to interpolate the Dirichlet data g on Γ_i. For problems with homogeneous data this definition gives the space $S_0^h(\Omega_i^h)$ consisting of piecewise linear functions that vanish on Γ_i, and which is a conforming approximation of $H^1_{\Gamma_i}(\Omega_i)$. $\{N_i^j\}_{j=1}^{n_i}$ is the standard nodal basis of $S^h(\Omega_i^h)$ with the property that

$$N_i^j(\boldsymbol{x}_k) = \delta_{jk} \quad \forall \boldsymbol{x}_k \in \mathcal{N}(\overline{\Omega}_i) \, . \tag{15}$$

A function $\phi_i^h \in S_g^h(\Omega_i^h)$ has the expansion

$$\phi_i^h = \sum_{j \in \mathcal{N}(\Omega_i) \cup \mathcal{N}(\Gamma_i^c)} c_i^j N_i^j + \sum_{j \in \mathcal{N}(\Gamma_i)} g(\boldsymbol{x}_j) N_i^j = \phi_{\Omega_i}^h + \phi_{\Gamma_i}^h \, . \tag{16}$$

where $\phi_{\Gamma_i}^h$ is the (piecewise linear) boundary interpolant of the Dirichlet data g. The function $\phi_{\Omega_i}^h$ is the part of ϕ_i^h that is unknown and must be determined.

The displacements $(\phi_1, \phi_2) \in \mathbf{H}_g$ for the mesh tying problem are approximated by the piecewise linear finite element space $\mathbf{H}_g^h = S_g^h(\Omega_1^h) \times S_g^h(\Omega_2^h)$. The space for homogeneous boundary conditions $\mathbf{H}_0^h = S_0^h(\Omega_1^h) \times S_0^h(\Omega_2^h)$ is a conforming approximation of $\mathbf{H}_0$. The product space $\mathbf{H}^h = S^h(\Omega_1^h) \times S^h(\Omega_2^h)$ is a conforming approximation of $\mathbf{H}$.

3.2.2 Approximation of the Lagrange multipliers

Formally, a conforming discretization of (7) requires a finite element subspace $\mathbf{D}^h$ of $H(\mathrm{div}, \Omega)$. For example, $\mathbf{D}^h$ can be the lowest order Raviart-Thomas space; see [2]. Of course, besides being utterly inefficient, such an implementation would require a conforming mesh on all of Ω, which defies the purpose of a mesh-tying method.

Fortunately, we won't need a finite element subspace of $H(\mathrm{div}, \Omega)$ because the Lagrange multiplier is unique up to an element of the space $\mathbf{Z}'$. It is easy to see that

$$\mathbf{Z}' = \{ \mathbf{w} \in H(\mathrm{div}, \Omega) \,|\, \mathbf{w} \cdot \boldsymbol{n} = 0 \ \text{ on } \Gamma_i^c, \, i = 1, 2 \} \, ,$$

and so, to discretize (7) we only need to approximate the traces of $\mathbf{w} \cdot \boldsymbol{n}$ rather than the field $\mathbf{w}$ itself.

We build the approximation space for the pair of traces $\{\mathbf{v} \cdot \boldsymbol{n}_1, \mathbf{v} \cdot \boldsymbol{n}_2\}$ in three stages. At the first stage we define the set

$$\mathbf{G}_L^h = \{ \overline{g}_c, \overline{g}_x, \overline{g}_y \}$$

where

$$\overline{g}_c = (0,0); \quad \overline{g}_x = (\mathbf{e}_1 \cdot \boldsymbol{n}_1, \mathbf{e}_1 \cdot \boldsymbol{n}_2); \quad \text{and} \quad \overline{g}_y = (\mathbf{e}_2 \cdot \boldsymbol{n}_1, \mathbf{e}_2 \cdot \boldsymbol{n}_2)$$

are piecewise constant functions with respect to the edges of Γ_i^c. From Lemma 2 we know that the pair $(\overline{\phi}^L, \nabla\overline{\phi}^L)$ satisfies the first two equations in (7). The functions included in $\mathbf{G}_L^h$ ensure that $\boldsymbol{n} \cdot \nabla\overline{\phi}^L$ are in the discrete Lagrange multiplier space so that $(\overline{\phi}^L, \nabla\overline{\phi}^L)$ will also solve the discretized equations (7), thus assuring passage of any linear patch test. Additional functions we add to the approximation space are not guaranteed to span the functions in $\mathbf{G}_L^h$, so we explicitly include them at this point. Further, we will force these additional functions to be consistent with a globally linear solution.

At the second stage we augment the piecewise constant space $\mathbf{G}_L^h$ by additional functions that are piecewise polynomials with respect to the interface segments. These polynomials are functions of the arc length along these segments and their degrees depend on the number of edges in the segments of Γ_i^c. Let $\dim \sigma_i^s$ be that number for σ_i^s. For every pair of segments $\{\sigma_1^s, \sigma_2^s\}$ we choose an integer number

$$0 \le r_s \le \min\{\dim \sigma_1^s \,, \dim \sigma_2^s\} - 1 \,,$$

and consider the space $\mathcal{P}_{r_s}(\sigma_i^s)$ of all polynomials of degree r_s or less, parameterized by the arc length along σ_i^s. The space

$$\mathbf{G}_r^h = \{(g_1^h, g_2^h) \,|\, g_i^h \in L^2(\Omega_i),\ g_i^h|_{\sigma_i^s} \in \mathcal{P}_{r_s}(\sigma_i^s)\ \forall \sigma_i^s \in \Gamma_i^c\} \,, \tag{17}$$

contains functions that are piecewise polynomials *with respect to the partition of* Γ_i^c *into segments* σ_i^s, that is,

$$g_i^h|_{\sigma_i^s} = \sum_{k=0}^{r_s} a_k(\sigma_i^s) t^k, \quad i = 1,2$$

where t is the arc length along segment σ_i^s and $a_k(\sigma_i^s)$ are real valued coefficients. On each pair of segments the local polynomial degree r_s is determined by the segment with the lesser number of edges, however, it does not have to be exactly equal to that number. In the extreme case when one of the segments σ_i^s consists of a single edge, $r_s = 0$ and $\{\mathbf{v} \cdot \boldsymbol{n}_1, \mathbf{v} \cdot \boldsymbol{n}_2\}$ are approximated by constants. The space (17) approximates functions in the dual spaces $H^{-1/2}(\Gamma_i^c)$ and so its elements are not subject to any boundary conditions.

Note that $\mathbf{G}_r^h$ contains pairs of piecewise polynomial functions that are defined independently of each other. On the other hand, the traces $\{\mathbf{v} \cdot \boldsymbol{n}_1, \mathbf{v} \cdot \boldsymbol{n}_2\}$ are not independent in the sense that they are obtained from the same vector field $\mathbf{v} \in H(\mathrm{div}, \Omega)$. At the third stage we account for this fact by selecting a subspace of $\mathbf{G}_r^h$ in which g_1^h and g_2^h are connected through their coefficients and the requirement that they are compatible with a linear patch test. This space is defined by the formula

$$\mathbf{G}_c^h = \{\overline{g}^h \in \mathbf{G}_r^h \,|\, \langle g_1^h, \phi_L\rangle_1 + \langle g_2^h, \phi_L\rangle_2 = 0;\ \ a_k(\sigma_1^s) = a_k(\sigma_2^s);\ 1 \le s \le n_\sigma;\ 0 \le k \le r_s\} \,, \tag{18}$$

where, as before, $\phi_L = ax + by + c$. The first constraint placed on $\overline{g}^h$ is necessary to ensure that linear functions will be admitted as solutions of the mesh tying problem, i.e., it makes the Lagrange multipliers *patch test consistent* [3] . The second condition in (18) simply states

[3] The space $\mathbf{G}_L^h$ is already patch test compatible. Indeed, $\overline{g}_0$ satisfies (18) trivially, and to see that $\overline{g}_x$ and $\overline{g}_y$ also satisfy this relation note that $g_x = (\partial x/\partial \boldsymbol{n}_1, \partial x/\partial \boldsymbol{n}_2)$, $g_y = (\partial y/\partial \boldsymbol{n}_1, \partial y/\partial \boldsymbol{n}_2)$ and the assertion follows from the arguments in Lemma 2.

that the g_1^h and g_2^h must have the same coefficients.

Lemma 3 *Let $r = \sum_{s=1}^{n_\sigma}(r_s+1)$. Dimension of $\mathbf{G}_c^h$ is greater than or equal to $r-3$ and less than r.*

Proof. Dimension of $\mathbf{G}_r^h$ equals $2r$. Enforcing the second constraint in (18) reduces this number to r. Then, it is easy to see that the patch test consistency condition

$$\langle g_1^h, \phi_L\rangle_1 + \langle g_2^h, \phi_L\rangle_2 = 0$$

is a $3\times r$ linear system whose rank is at least 1 and at most 3. Thus, $r-3 \le \dim \mathbf{G}_c^h < r$. □

To complete the construction of the discrete Lagrange multiplier space we set

$$\mathbf{G}^h = \mathbf{G}_L^h \cup \mathbf{G}_c^h\,. \tag{19}$$

Remark 1 *The functions $\overline{g}_x$ and $\overline{g}_y$ from $\mathbf{G}_L^h$ are piecewise constants with respect to the partition of Γ_i^c into edges. In contrast, the polynomials in $\mathbf{G}_c^h$ are parameterized by the arc length of the segments in Γ_i^h. As a result, unless interface segments coincide with the finite element edges, $\mathbf{G}_L^h \cap \mathbf{G}_c^h = \emptyset$ and $\overline{g}_x$ and $\overline{g}_y$ are not in $\mathbf{G}_c^h$. For this reason, $\overline{g}_x$ and $\overline{g}_y$ must be added explicitly to the definition of the Lagrange multiplier space in (19).*

3.3 Discrete equations

To discretize (7) and define the finite element mesh tying problem we use the spaces $\mathbf{H}_g^h$ and $\mathbf{G}^h$. The discrete equations are: seek $\overline{\phi}^h \in \mathbf{H}_g^h$ and $\overline{g}^h \in \mathbf{G}^h$ such that

$$\begin{aligned}
\left(\nabla\phi_1^h, \nabla\psi_1^h\right) \qquad\qquad -\langle g_1^h, \psi_1^h\rangle_1 &= \left(f, \psi_1^h\right) \quad \forall \psi_1^h \in S_{\Gamma_1}^h(\Omega_1)\\
\left(\nabla\phi_2^h, \nabla\psi_2^h\right) -\langle g_2^h, \psi_2^h\rangle_2 &= \left(f, \psi_2^h\right) \quad \forall \psi_2^h \in S_{\Gamma_2}^h(\Omega_2)\\
\langle q_1^h, \phi_1^h\rangle_1 \quad +\langle q_2^h, \phi_2^h\rangle_2 &= 0 \qquad\quad \forall \overline{q}^h \in \mathbf{G}^h
\end{aligned} \tag{20}$$

For the subdomain displacements we have the standard nodal basis defined in (15). After selecting a basis $\{\overline{\Lambda}^l\} = \{(\Lambda_1^l, \Lambda_2^l)\}$ for $\mathbf{G}^h$,

$$\overline{g}^h = \sum_{k=1}^{\dim \mathbf{G}^h} \gamma_k \overline{\Lambda}^k = \sum_{k=1}^{\dim \mathbf{G}^h} \gamma_k \left(\Lambda_1^k, \Lambda_2^k\right)$$

and it is easy to see that problem (20) is equivalent to the linear system of algebraic equations

$$\begin{aligned}
\mathbb{K}^1\phi_{\Omega_1}^h \qquad\quad + (\mathbb{C}^1)^T g^h &= \mathbf{f}_1 - \mathbb{B}^1\phi_{\Gamma_1}^h\\
\mathbb{K}^2\phi_{\Omega_2}^h + (\mathbb{C}^2)^T g^h &= \mathbf{f}_2 - \mathbb{B}^2\phi_{\Gamma_2}^h\\
\mathbb{C}^1\phi_{\Omega_1}^h + \mathbb{C}^2\phi_{\Omega_2}^h \qquad &= -\mathbb{D}^1\phi_{\Gamma_1}^h - \mathbb{D}^2\phi_{\Gamma_2}^h
\end{aligned} \tag{21}$$

for the unknown coefficients $\phi_{\Omega_1}^h$, $\phi_{\Omega_2}^h$ of the subdomain displacements, and the unknown coefficients $g^h = (\gamma_1, \ldots, \gamma_k)$, of the interface fluxes.

In practice, the last equation in (20) requires the constraint integrals to be done exactly. For the functions in $\mathbb{G}_L^h$, closed-form expressions for the exact integrals can be easily derived. Since the only functions in $\mathbb{G}_c^h$ are patch-test consistent polynomials of degree at most r_s, we can economically compute exact integrals by performing a Gaussian quadrature that is exact up to degree at most $r_s + 1$, where we take the shape functions to be linear polynomials.

The matrices in (20) are defined in the usual manner by

$$\mathbb{K}_{kj}^i = \left(\nabla N_i^j, \nabla N_i^k\right) \; k, j \in \mathcal{N}(\Omega_i) \cup \mathcal{N}(\Gamma_i^c)$$

$$\mathbb{B}_{kj}^i = \left(\nabla N_i^j, \nabla N_i^k\right) \; k \in \mathcal{N}(\Omega_i) \cup \mathcal{N}(\Gamma_i^c) \text{ and } j \in \mathcal{N}(\Gamma_i)$$

$$\mathbb{C}_{lj}^i = \langle \Lambda_i^l, N_i^j \rangle_i \qquad l = 1, \ldots \dim(\mathbb{G}^h) \text{ and } j \in \mathcal{N}(\Omega_i) \cup \mathcal{N}(\Gamma_i^c)$$

$$\mathbb{D}_{kj}^i = \langle \Lambda_i^l, N_i^j \rangle_i \qquad l = 1, \ldots \dim(\mathbb{G}^h) \text{ and } j \in \mathcal{N}(\Gamma_i)$$

4 Numerical results

In this section we present numerical results that demonstrate the accuracy of the new mesh-tying method and its ability to pass a linear patch test for non-coincident interfaces. To verify that the method passes a linear patch test we set

$$\phi(x, y) = x + y + 1 \,. \tag{22}$$

while to assess the order of accuracy of our method in L^2 and H^1 norms we use the exact solution given by

$$\phi(x, y) = (x^2 + y^2) \cos\left(2 \arctan(y/x)\right) \,. \tag{23}$$

In addition, we also compare the L^2 and H^1 errors of the two-domain solution obtained by the new method for *non-matching* and *matching* interfaces with the errors of a standard Ritz-Galerkin method on a single domain.

4.1 Example domains 1 and 2

In this section we use the example domains from Fig. 1. In example domain 1 (annulus), the two-domain problem with noncoincident mesh has four times as many edges on the "fine" side as the "coarse" side. In example domain 2 (unit square), the two-domain problem with noncoincident mesh has two times as many edges on the "fine" side as the "coarse" side.

We begin by setting the right hand side and boundary data function in (1) to be consistent with the linear solution (22). The finite element approximation of this function, computed by the mesh tying method, is shown in Fig. 4. In both cases, the linear solution is recovered exactly and so, we can conclude that the mesh-tying method passes the linear patch test. It is worth mentioning that in order to pass the patch test it suffices to choose $\mathbf{G}^h = \mathbf{G}_L^h$, so long as there are no "floating" subdomains. The reason for this is that $\mathbf{G}_L^h$ contains all

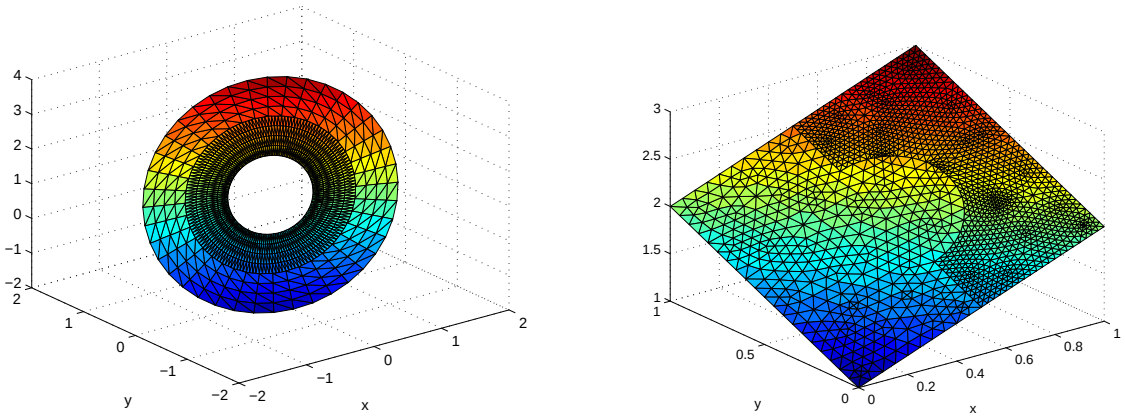

(a) Example 1. (b) Example 2.

Fig. 4. Finite element approximation of (22) by the mesh-tying method. The linear function is recovered exactly in both cases.

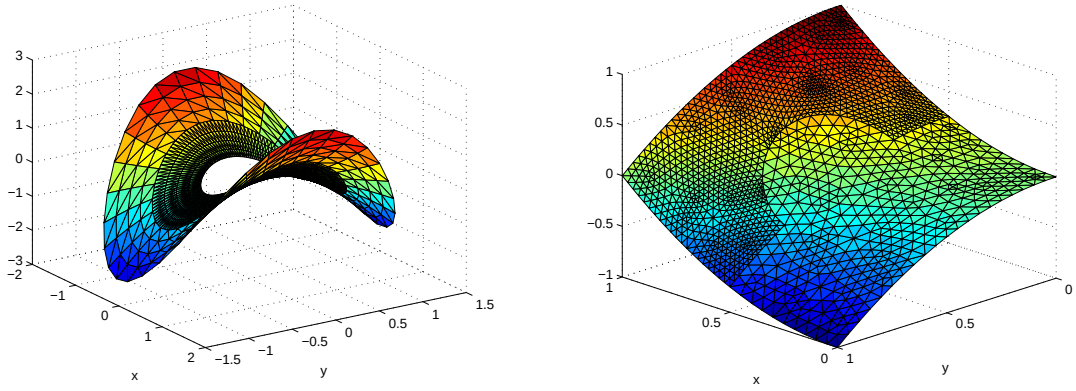

(a) Example 1. (b) Example 2.

Fig. 5. Finite element approximation of (23) by the mesh-tying method.

information needed to recover exactly the flux of any linear function on the interfaces. In the presence of a floating subdomain, any single additional polynomial-type constraint is sufficient to resolve the zero-energy mode. We discuss the solution of problems with floating subdomains further in §4.2.

Of course, in the general case, the set $\mathbf{G}_L^h$ alone will not be enough to provide sufficiently accurate solutions. Thus, to carry out the order of accuracy studies we define $\mathbf{G}^h$ from Eqn. 19 by using the procedure described in §3.2.2. We choose the piecewise polynomial space $\mathcal{P}_{r_s}(\sigma_i^s)$ (with respect to the segment partition) to be the set of Legendre polynomials of degree r_s and lower defined over the segment σ_i^s. In general, to avoid ill-conditioning of the the matrices $\mathbb{C}^1$ and $\mathbb{C}^2$ in (21), we will want to choose an orthogonal polynomial basis over each segment σ_i^s; the Legendre polynomials are one such basis. We note that in general, the number of constraints is far less than the number of edges along the contact boundaries.

The specific choice of $\mathbb{G}^h$ in (19) for our two examples deserves some discussion. For example domain 1 (annulus), we have only one contact interface segment (see figure 2(a)), and we chose $r_1 = 19$ in (17) for all cases, as shown in tables 1 and 2. That is, the first 20 Legendre

polynomials were used, and the three of highest degree were discarded when defining (18). Combined with the two constraints in $\mathbb{G}_L^h$, 19 total constraints were used. For example domain 2 (unit square), there are three contact interface segments (see figure 2(b)). For simplicity, we chose $r_1 = r_2 = r_3$. On segments σ_1 and σ_2, we see that the boundaries are straight and vertical. This means that for $\mathbb{G}_L^h$, we have that $\overline{g}_x = \overline{g}_c$ and thus we need not enforce $\overline{g}_x$ explicitly. We also see that $\overline{g}_y$ is constant, and thus dependant with a constant (degree zero) polynomial-type constraint in $\mathbb{G}_r^h$ in (17). Thus, on these two segments, we discard the patch test constraints $\mathbb{G}_L^h$ completely (see also the comments made in Remark 1). The segment σ_3 requires no special treatment because it is curved and thus has none of these issues. As the mesh for this example is refined, the number of edges along the contact boundary segments increases, and we increase the polynomial degrees r_1, r_2, r_3 in (17) accordingly, as shown in tables 3 and 4.

In the tables and figures below, h_{max} is defined as the length of the longest edge in the computational domain, and $\mathcal{N}_e(\Omega)$ is the number of elements in domain Ω. For problems where we join a "fine" and a "coarse" mesh, the longest edge is always in the "coarse" region.

Fig. 5 shows plots of the finite element approximation of (23) computed by the mesh-tying method for the two example domains. We then proceed to solve three different configurations of (1) on a sequence of refined grids. Specifically, we use a standard Ritz-Galerkin method on a single domain, and the mesh-tying method on two subdomains with both matching and non-matching interfaces. Plots of the H^1 and L^2 errors for the two example domains and the three different problem configurations are shown in figures 6 and 7, respectively. Several conclusions can be drawn from these figures. First, we see that the errors for the matching and non-matching interface cases are basically identical. This means that the new mesh-tying method is applicable to virtually any possible interface configuration. Second, the lines connecting the L^2 and H^1 errors have slopes approximately equal to 2 and 1, respectively, which means that our method also converges at the best possible rate. These conclusions are further confirmed by the error data collected in Tables 1-4.

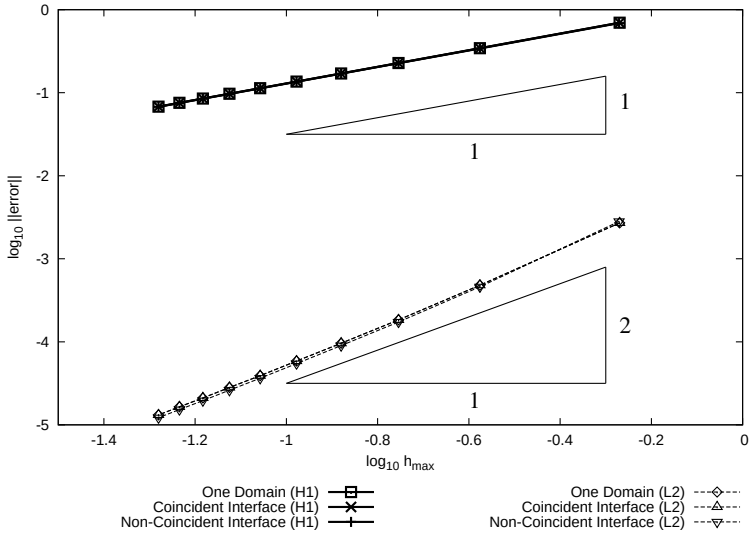

Fig. 6. Plot of the L^2 and H^1 errors for example 1 (annulus) obtained by a standard Galerkin solution on a single domain and the mesh-tying method with both coincident and noncoincident interfaces. Data from this figure is tabulated in Tables 1 and 2.

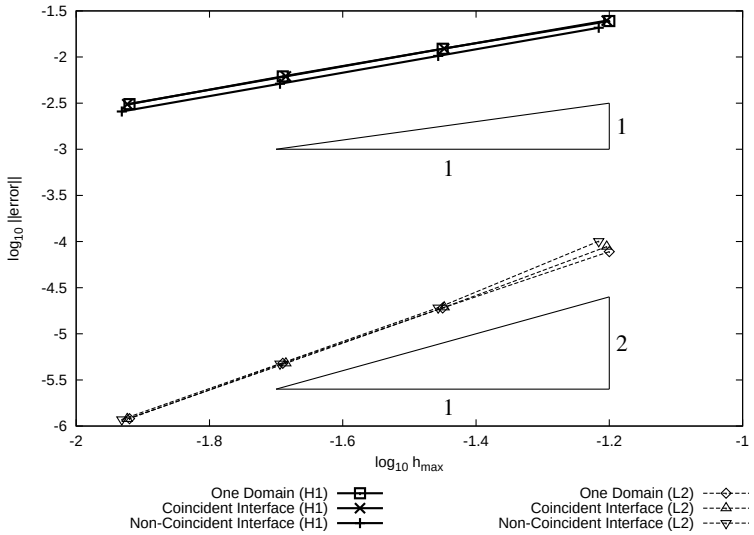

Fig. 7. Plot of the L^2 and H^1 errors for example 2 (unit square) obtained by a standard Galerkin solution on a single domain and the mesh-tying method with both coincident and noncoincident interfaces. Data from this figure is tabulated in Tables 3 and 4.

One-domain				Two-domain (coincident interface)					
$\mathcal{N}_e(\Omega)$	h_{max}	H^1	L^2	$\mathcal{N}_e(\Omega_1)$	$\mathcal{N}_e(\Omega_2)$	$\dim \mathbf{G}^h$	h_{max}	H^1	L^2
156	5.37E-01	6.97E-01	2.71E-03	78	78	19	5.37E-01	6.97E-01	2.71E-03
768	2.66E-01	3.44E-01	4.80E-04	384	384	19	2.66E-01	3.44E-01	4.80E-04
1872	1.76E-01	2.28E-01	1.84E-04	936	936	19	1.76E-01	2.28E-01	1.84E-04
3456	1.32E-01	1.71E-01	9.62E-05	1728	1728	19	1.32E-01	1.71E-01	9.62E-05
5540	1.05E-01	1.36E-01	5.86E-05	2770	2770	19	1.05E-01	1.36E-01	5.86E-05
8136	8.76E-02	1.13E-01	3.92E-05	4068	4068	19	8.76E-02	1.13E-01	3.92E-05
11200	7.50E-02	9.72E-02	2.81E-05	5600	5600	19	7.50E-02	9.72E-02	2.81E-05
14784	6.56E-02	8.50E-02	2.11E-05	7392	7392	19	6.56E-02	8.50E-02	2.11E-05
18828	5.83E-02	7.55E-02	1.65E-05	9414	9414	19	5.83E-02	7.55E-02	1.65E-05
23400	5.24E-02	6.79E-02	1.32E-05	11700	11700	19	5.24E-02	6.79E-02	1.32E-05

Table 1
Convergence history for example 1 (annulus) comparing the one-domain solution with solution by mesh-tying algorithm for the case of coincident interfaces. In this case, the finite element meshes for the one-domain and two-domain problems are identical, hence $\mathcal{N}_e(\Omega) = \mathcal{N}_e(\Omega_1) + \mathcal{N}_e(\Omega_2)$. The H^1 and L^2 errors for the one and two-domain models here are essentially identical, and are plotted in Fig. 6.

4.2 Floating subdomains

In this section we use the example domain from Fig. 8, which includes the "floating" subdomain Ω_1. The purpose of this section is to confirm experimentally that floating subdomains do not pose any difficulty for our proposed mesh-tying method. We consider a noncoincident mesh where the "fine" side has four times as many edges as the "coarse" side.

As with the previous section, we first demonstrate passage of the patch test problem (22). The solution is recovered exactly, and is shown in Fig. 9(a). For this example, we have only one contact interface segment σ_1 (see figure 2(a)), and we choose $r_1 = 3$ in (17), so that $\dim \mathbb{G}_c^h = 1$. The space $\mathbb{G}_c^h$ is sufficient to resolve the zero-energy mode of the floating

One-domain				Two-domain (non-coincident interface)					
$\mathcal{N}_e(\Omega)$	h_{max}	H^1	L^2	$\mathcal{N}_e(\Omega_1)$	$\mathcal{N}_e(\Omega_2)$	$\dim \mathbf{G}^h$	h_{max}	H^1	L^2
156	5.37E-01	6.97E-01	2.71E-03	78	312	19	5.36E-01	6.88E-01	2.82E-03
768	2.66E-01	3.44E-01	4.80E-04	384	1536	19	2.66E-01	3.41E-01	4.60E-04
1872	1.76E-01	2.28E-01	1.84E-04	936	3744	19	1.76E-01	2.27E-01	1.73E-04
3456	1.32E-01	1.71E-01	9.62E-05	1728	6912	19	1.32E-01	1.70E-01	8.99E-05
5540	1.05E-01	1.36E-01	5.86E-05	2770	11080	19	1.05E-01	1.36E-01	5.46E-05
8136	8.76E-02	1.13E-01	3.92E-05	4068	16272	19	8.76E-02	1.13E-01	3.64E-05
11200	7.50E-02	9.72E-02	2.81E-05	5600	22400	19	7.50E-02	9.67E-02	2.61E-05
14784	6.56E-02	8.50E-02	2.11E-05	7392	29568	19	6.56E-02	8.46E-02	1.96E-05
18828	5.83E-02	7.55E-02	1.65E-05	9414	37656	19	5.83E-02	7.51E-02	1.53E-05
23400	5.24E-02	6.79E-02	1.32E-05	11700	46800	19	5.24E-02	6.76E-02	1.22E-05

Table 2
Convergence history for example 1 (annulus) comparing the one-domain solution with solution by mesh-tying algorithm for the case of non-coincident interfaces. In this case, the meshes for the one-domain and two-domain models are different. Because the mesh in the domain Ω_2 is finer in the two-domain model than for the corresponding region in the one-domain model, we expect the H^1 errors to be slightly smaller in the two-domain model. The H^1 and L^2 errors for the one and two-domain models here are plotted in Fig. 6.

One-domain				Two-domain (coincident interface)					
$\mathcal{N}_e(\Omega)$	h_{max}	H^1	L^2	$\mathcal{N}_e(\Omega_1)$	$\mathcal{N}_e(\Omega_2)$	$\dim \mathbf{G}^h$	h_{max}	H^1	L^2
1408	6.25E-02	2.48E-02	7.74E-05	840	568	18	6.25E-02	2.48E-02	8.80E-05
5632	3.57E-02	1.23E-02	1.92E-05	3360	2272	36	3.57E-02	1.23E-02	1.94E-05
22528	2.06E-02	6.16E-03	4.78E-06	13440	9088	42	2.06E-02	6.16E-03	4.78E-06
90112	1.19E-02	3.08E-03	1.19E-06	53760	36352	48	1.19E-02	3.08E-03	1.19E-06

Table 3
Convergence history for example 2 (unit square) comparing the one-domain solution with solution by mesh-tying algorithm for the case of coincident interfaces. In this case, the finite element meshes for the one-domain and two-domain problems are identical, hence $\mathcal{N}_e(\Omega) = \mathcal{N}_e(\Omega_1) + \mathcal{N}_e(\Omega_2)$. The H^1 and L^2 errors for the one and two-domain models here are essentially identical, and are plotted in Fig. 7.

One-domain				Two-domain (non-coincident interface)					
$\mathcal{N}_e(\Omega)$	h_{max}	H^1	L^2	$\mathcal{N}_e(\Omega_1)$	$\mathcal{N}_e(\Omega_2)$	$\dim \mathbf{G}^h$	h_{max}	H^1	L^2
1408	6.25E-02	2.48E-02	7.74E-05	840	2272	18	6.08E-02	2.07E-02	1.01E-04
5632	3.57E-02	1.23E-02	1.92E-05	3360	9088	36	3.49E-02	1.03E-02	1.92E-05
22528	2.06E-02	6.16E-03	4.78E-06	13440	36352	42	2.02E-02	5.14E-03	4.75E-06
90112	1.19E-02	3.08E-03	1.19E-06	53760	145408	48	1.17E-02	2.57E-03	1.18E-06

Table 4
Convergence history for example 2 (unit square) comparing the one-domain solution with solution by mesh-tying algorithm for the case of non-coincident interfaces. In this case, the meshes for the one-domain and two-domain models are different. Because the mesh in the domain Ω_2 is finer in the two-domain model than for the corresponding region in the one-domain model, we expect the H^1 errors to be slightly smaller in the two-domain model. The H^1 and L^2 errors for the one and two-domain models here are plotted in Fig. 7.

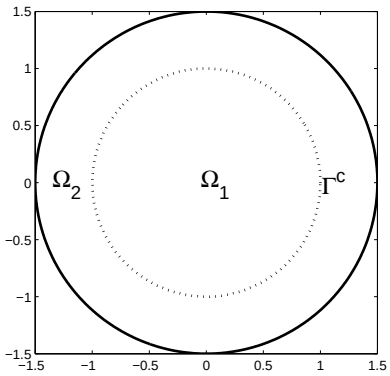

Fig. 8. Computational domain with floating subdomain Ω_1.

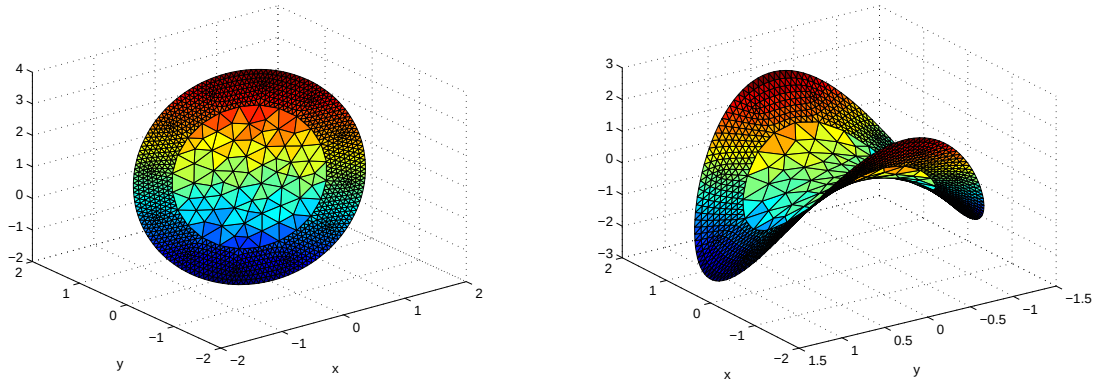

(a) Eqn. (22) (Patch test). (b) Eqn. (23).

Fig. 9. Finite element solutions of (22) and (23) on the domain in Fig. 8 by the mesh-tying method.

subdomain, and the space $\mathbb{G}_L^h$, is sufficient to resolve exactly a globally linear solution.

The finite element approximation of (23) on this domain by the mesh-tying method is shown in Fig. 9(b), where the computed errors are in agreement with those of a standard Ritz-Galerkin method on a single domain. For this problem, we must choose $\mathbb{G}^h$ (and thus $\mathbb{G}_r^h$) to be of larger dimension. In (17), we selected $r_1 = 19$, meaning that in $\mathbb{G}_c^h$ (after enforcing patch test consistency) the first 17 Legendre polynomials were used. Coupled with the two constraints from $\mathbb{G}_L^h$, there were 19 constraints total.

5 Concluding remarks

In this paper we proposed and studied a new method for tying computational domains with non-matching interfaces. Our mesh-tying algorithm is based on the idea of equilibrating weighted solution averages on the segments of the non-matching interfaces. The method uses a discrete constraint space defined by augmenting a basic constraint space that represents exactly fluxes of linear functions by a higher order, piecewise polynomial (with respect to the segments of the interface) space. The method can be viewed as a discretization of a formal, well-posed variational formulation for non-matching interface problems, in which continuity constraints are imposed by using the trace of the normal component of a globally defined

vector field.

We show that a necessary condition for passing a linear patch test is cancellation of the areas of the void and overlap regions created by the non-matching interfaces. As a result, in conjunction with an interface balancing procedure to satisfy this condition, our method passes a linear patch test. The accuracy of the method agrees with that of a standard Galerkin formulation on a single domain for both matching and non-matching interfaces. Rigorous error analysis, extension to a higher order patch test and linear elasticity will be reported in a forthcoming paper.

Acknowledgments

During the preparation of this work we benefited from many helpful discussions with David Day, Clark Dohrman, Michael Gee, Martin Heinstein, Sam Key, and Barbara Wohlmuth. Their valuable help and insight are greatly appreciated.

References

[1] F. Brezzi. On existence, uniqueness and approximation of saddle-point problems arising from Lagrange multipliers. *Model. Math. Anal. Numer.*, 21:129–151, 1974.

[2] F. Brezzi and M. Fortin. *Mixed and Hybrid Finite Element Methods*. Springer, Berlin, 1991.

[3] C. R. Dohrmann, S. W. Key, and M. W. Heinstein. A method for connecting dissimilar finite element meshes in two dimensions. *Int. J. Numer. Meth. Engng.*, 48:655–678, 2000.

[4] C. R. Dohrmann, S. W. Key, and M. W. Heinstein. Methods for connecting dissimilar three-dimensional finite element meshes. *Int. J. Numer. Meth. Engng.*, 47:1057–1080, 2000.

[5] C. Farhat and F.-X. Roux. A Method of Finite Element Tearing and Interconnecting and its Parallel Solution Algorithm. *Int. J. Numer. Meth. Engrg.*, 32, 1991.

[6] B. Flemisch, J.M. Melenk, and B.I. Wohlmuth. Mortar methods with curved interfaces. *Appl. Numer. Math.*, 54(3-4):339–361, 2005.

[7] B. Flemisch, M.A. Puso, and B.I. Wohlmuth. A new dual mortar method for curved interfaces: 2D elasticity. *Internat. J. Numer. Methods Engrg.*, 63(6):813–832, 2005.

[8] Bernd Flemisch and Barbara I. Wohlmuth. Stable lagrange multipliers for quadrilateral meshes of curved interfaces in 3D, IANS preprint 2005/005. Technical report, University of Stuttgart, 2005.

[9] V. Girault and P. Raviart. *Finite Element Methods for Navier-Stokes Equations*. Springer, Berlin, 1986.

[10] M. W. Heinstein and T. A. Laursen. A three dimensional surface-to-surface projection algorithm for non-coincident domains. *Commun. Numer. Meth. Engng.*, 19:421–432, 2003.

[11] T. A. Laursen and M. W. Heinstein. Consistent mesh tying methods for topologically distinct discretized surfaces in non-linear solid mechanics. *Int. J. Numer. Meth. Engng.*, 57:1197–1242, 2003.

[12] A. Toselli and O. Widlund. *Domain decomposition methods - algorithms and theory*. Springer Verlag, 2005.